Statistical analysis of the chaotic optical field from a self-amplified spontaneous-emission free-electron laser

S. Krinsky
NSLS, Brookhaven National Laboratory, Upton, New York 11973, USA

Y. Li
Advanced Photon Source, Argonne National Laboratory, Argonne, Illinois 60439, USA

(Received 4 January 2006; published 6 June 2006)

We use Rice's theory of shot noise random processes to provide a statistical analysis of the evolution of the amplitude and phase of the chaotic optical field from a high-gain, self-amplified, spontaneous-emission (SASE) free-electron laser. The theoretical framework developed is compared with recent frequency-resolved optical-gating measurements of the SASE output at the LEUTL facility at Argonne National Laboratory.

DOI: 10.1103/PhysRevE.73.066501 PACS number(s): 41.60.Cr, 42.50.Ar, 05.40.−a, 42.55.Vc

I. INTRODUCTION

A high-gain, self-amplified, spontaneous-emission (SASE) free-electron laser [1,2] (FEL), based on modern beam technology, has the advantage of operating without a resonator and hence is capable of generating coherent radiation with wavelength down to the x-ray region. There are two systems under construction for 1.5–1 Å radiation [3,4] and a host of application experiments utilizing the high-intensity and short-pulse capability have been planned.

The gain in a FEL is based on the constructive growth of an instability in an electron beam when it is propagating down a stream of undulators. The "microbunching instability" grows as the result of an interaction between the electron beam and the electromagnetic wave it emits as it traverses the magnetic field of the undulator. The instability modulates the electron density on the scale of the radiation wavelength resulting in coherent radiation. Provided that the instability is strong enough, the radiation grows exponentially before reaching saturation [5–7]. The wavelength of a FEL is determined by the resonance frequency

$$\omega_r = \frac{4\pi c\gamma^2}{\lambda_u(1+K^2/2)}. \tag{1.1}$$

Here γ is the relativistic factor of the beam, and λ_u and K are, respectively, the undulator period and field strength parameter. For 1 Å operation, with $\lambda_u=3.3$ cm and $K=3.1$, the relativistic parameter $\gamma\sim 30\,000$, corresponding to a beam energy of 15 GeV, accessible to modern accelerators.

Chaotic light is normally produced by incoherent light sources such as the sun or incandescent light bulbs, and has long been the subject of statistical optics [8]. All naturally occurring chaotic light sources have large spectral bandwidth and large divergence angle, meaning poor longitudinal and transverse coherence. When filtered to proper temporal and spatial coherence, the intensity is too low to allow time-resolved measurements. Therefore, until now statistical optics has mainly been studied in a time-integrated and ensemble-averaged fashion, as in the famous Hanbury-Brown and Twiss experiment [9]. The SASE FEL is a unique chaotic light source because of its excellent transverse coherence and high intensity. It provides a new opportunity for study of the dynamics of statistical optics, including measurement of the evolution of the phase as well as the amplitude using well-developed light-characterizing techniques such as frequency-resolved optical gating (FROG) [10].

As we have noted, the SASE FEL starts up from the shot noise in the electron beam [11,12]. The temporal behavior of the system is that of a narrowband amplifier with a broadband Poisson seed. Before saturation the output is a Gaussian random process and the radiated field is chaotic, quasimonochromatic, polarized light. Near saturation, the transverse behavior of the output is dominated by an intense, single spatial mode. Ignoring the transverse dependence, the radiated electric field can be expressed in the form

$$E(z,t) = A(z,t)\exp(ik_r z - i\omega_r t), \tag{1.2}$$

where z represents the location along the undulator at which the SASE is observed and t represents the temporal position in the radiation pulse. In the case of a cold electron beam with a long, flat-top electron bunch profile, the SASE field before saturation is the superposition of many electromagnetic wave packets emitted from randomly distributed, individual electrons. Within the classical, one-dimensional theory, the slowly varying envelope can be approximated by

$$A(z,t) \cong A_0(z)\sum_{j=1}^{N_e} \exp\left[i\omega_r t_j - \frac{(t-t_j-z/v_g)^2}{4\sigma^2}\left(1+\frac{i}{\sqrt{3}}\right)\right], \tag{1.3}$$

where N_e is the total number of electrons in the bunch, $A_0(z)$ contains the exponential growth factor, t_j is the random arrival time of the jth electron at the undulator entrance, and v_g is the group velocity of each wave packet. The characteristic wave packet width $\sigma=1/(\sqrt{3}\sigma_\omega)$, where $\sigma_\omega=\omega_r\sqrt{3\sqrt{3}\rho_p/k_u z}$ is the SASE bandwidth [11,12] and ρ_p the FEL Pierce parameter [2].

The field amplitude (1.3) is expressed as a sum of independent random terms. Rice [13] has developed a comprehensive method to analyze such sums using the central limit theorem. Although his work was motivated by the study of

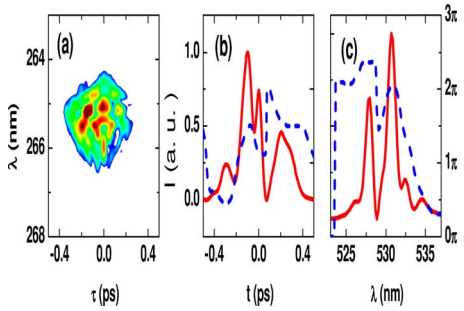

FIG. 1. (Color online) (a) Typical raw FROG data and the retrieved field intensity (red, solid) and phase (blue, dashed) as a function of time (b) and wavelength (c) of the SASE output. See Sec. IV for more details.

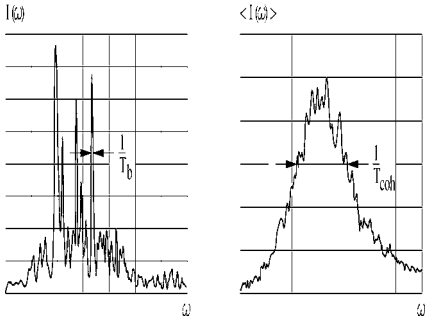

FIG. 2. Schematic of intensity spiking in the frequency domain (arbitrary units). In the single-shot spectrum shown on the left, the width of the peaks is inversely proportional to the electron bunch duration T_b. The average of many SASE pulses is illustrated on the right, and in this case the width is proportional to the gain bandwidth $\sigma_\omega = \sqrt{\pi}/T_{\mathrm{coh}}$.

shot noise in electrical circuits, his approach has found important application in statistical optics [8] and, in particular, in the description of the chaotic output of the SASE FEL [14,15]. Recently, FROG was used to characterize the temporal evolution of the chaotic SASE output [16,17], and the experimental results were found to be in agreement with the predictions of analytic theory as well as numerical simulation. In this paper, we apply Rice's statistical description of intensity peaks and valleys to SASE and derive the analytic results reported in Refs. [16,17]. Our analysis extends the earlier work presented in Ref. [15].

As illustrated in Fig. 1, the FEL output intensity as a function of time exhibits spiking [18]. The width of the intensity spikes is characterized by the coherence time [14,15]. We note that the phase change is small near the intensity maxima but can be larger near the intensity minima. The rapid phase variation at the minima is closely related to the loss of temporal coherence between spikes.

In this paper, we derive distributions for the peak intensity, temporal width, frequency (phase derivative), and frequency chirp (phase second derivative) at intensity maxima. The corresponding distributions characterizing intensity minima can also be determined. In particular, we discuss the frequency distribution at the intensity minima, which is found to be much broader than the frequency distribution at the intensity maxima. This is related to the loss of coherence between spikes.

Our paper is organized as follows: In Sec. II, for the case of a long electron bunch of constant density, we describe the statistical properties of the SASE output using the analysis of shot noise random processes developed by Rice [13]. In Sec. III, we discuss the case of a Gaussian-distributed electron density. We show that although there is no time translation invariance, the statistical behavior of the chaotic electric field can be determined in terms of a stationary Gaussian random process. In Sec. IV, we compare our theoretical results with experiments [16,17] that were carried out at the LEUTL facility at Argonne National Laboratory. Some concluding remarks are given in Sec. V. In the Appendix, we provide a review of Rice's derivation of the distribution describing the statistical properties of intensity peaks and valleys.

II. STATISTICAL DESCRIPTION OF SASE BASED ON ANALYSIS OF RICE

In the absence of an external seed laser, the SASE FEL starts up from the shot noise in the electron beam. To describe the shot noise, one considers the arrival time of the individual electrons at the undulator entrance to be independent random variables, and one determines the statistical properties of the output radiation by averaging over the stochastic ensemble of arrival times. In the linear regime before saturation, it follows from the central limit theorem [13] that the probability distribution describing the spectral intensity $I(\omega)$, or the time-domain intensity $I(t)$, is the negative exponential distribution [8,14]

$$p_I(I) = \frac{1}{\langle I \rangle} e^{-I/\langle I \rangle}, \tag{2.1}$$

and the intensity fluctuation is 100%. The angular brackets indicate an ensemble average over the arrival times.

The output intensity as a function of time exhibits spiking [18] (see Fig. 1), and the width of the intensity peaks is characterized by the coherence time [14,15] $T_{\mathrm{coh}} = \sqrt{\pi}/\sigma_\omega$, where σ_ω is the SASE gain bandwidth. The spectral intensity also exhibits spikes (Fig. 2), and the width of the spectral peaks is inversely proportional to the electron bunch duration T_b.

At a fixed position z along the undulator, consider the energy in a single SASE pulse,

$$W(z) \propto \int_0^{T_b} |E(t,z)|^2 dt, \tag{2.2}$$

where T_b is the duration of an electron bunch having uniform average density. For z fixed, one can think of dividing the pulse into M statistically independent time intervals of width T_{coh}. The energy fluctuation within a single coherent region is 100%, but the fluctuation σ_W/W of the energy in the entire pulse is reduced and given by [8]

$$\frac{\sigma_W^2}{W^2} = \frac{\langle (W - \langle W \rangle)^2 \rangle}{\langle W \rangle^2} \equiv \frac{1}{M} \equiv \frac{T_{\mathrm{coh}}}{T_b}. \tag{2.3}$$

Here, M is defined [8] to be the number of modes in the radiation pulse. The energy per pulse is described by the Γ distribution [13]

$$p_W(W) = \frac{M^M}{\Gamma(M)} \left(\frac{W}{\langle W \rangle} \right)^{M-1} \frac{1}{\langle W \rangle} \exp\left(-M \frac{W}{\langle W \rangle} \right). \tag{2.4}$$

As in Eq. (1.2), let $E(z,t) = A(z,t)\exp(ik_r z - i\omega_r t)$ be the radiated SASE electric field. In the description (at fixed z) of the statistical properties of the SASE output, two important quantities are the field correlation function

$$g_1(t_1 - t_2) = \frac{\langle A(t_1) A^*(t_2) \rangle}{\sqrt{\langle |A(t_1)|^2 |A(t_2)|^2 \rangle}} \tag{2.5}$$

and the intensity correlation function

$$g_2(t_1 - t_2) = \frac{\langle |A(t_1)|^2 |A(t_2)|^2 \rangle}{\langle |A(t_1)|^2 \rangle \langle |A(t_2)|^2 \rangle}. \tag{2.6}$$

Here we do not explicitly show the dependence of the field on z. In the linear region before saturation [14],

$$g_2(t) = 1 + |g_1(t)|^2. \tag{2.7}$$

The energy fluctuation σ_W in a pulse can be expressed in the form

$$\frac{\sigma_W^2}{W^2} = \frac{1}{T_b^2} \int_0^{T_b} dt_1 \int_0^{T_b} dt_2 [g_2(t_1 - t_2) - 1] = \frac{1}{T_b} \int_{-T_b}^{T_b} dt |g_1(t)|^2. \tag{2.8}$$

Comparing Eqs. (2.3) and (2.8), we see that (when $T_{\mathrm{coh}} \ll T_b$) the coherence time can be expressed in terms of the field correlation function according to [8]

$$T_{\mathrm{coh}} = \int dt |g_1(t)|^2. \tag{2.9}$$

A useful approximation is [14,15]

$$g_1(t) = \exp\left(-\frac{\sigma_\omega^2 t^2}{2} \right), \tag{2.10}$$

in which case it follows from (2.9) that

$$T_{\mathrm{coh}} = \frac{\sqrt{\pi}}{\sigma_\omega}. \tag{2.11}$$

In the time domain, the joint probability that at a fixed position z along the undulator axis, the normalized intensity $Q \equiv I/\langle I \rangle$ in the radiation pulse has the values Q_1 and Q_2 at times t_1 and t_2 is given by [13,15]

$$P(Q_1, Q_2) = \frac{e^{-Q_1/(1-\beta_{12})} e^{-Q_2/(1-\beta_{12})}}{1 - \beta_{12}} I_0\left(\frac{2\sqrt{\beta_{12} Q_1 Q_2}}{1 - \beta_{12}} \right), \tag{2.12}$$

where

$$\beta_{12} = g_2(t_1 - t_2) - 1 = e^{-\sigma_\omega^2 (t_1 - t_2)^2}. \tag{2.13}$$

The conditional average $\langle Q_2 \rangle_{Q_1}$ of the intensity at t_2, given that the intensity at t_1 is Q_1, is given by [15]

$$\langle Q_2 \rangle_{Q_1} = \frac{\int_0^\infty dQ_2 Q_2 P(Q_1, Q_2)}{\int_0^\infty dQ_2 P(Q_1, Q_2)} = Q_1 + (1 - \beta_{12})(1 - Q_1). \tag{2.14}$$

We note from Eq. (2.14) that $\langle Q_2 \rangle_{Q_1}$ is less than Q_1 when $Q_1 > 1$, and is greater than Q_1 when $Q_1 < 1$. This is the statistical basis for the appearance of spikes in the radiation output. A reasonable approximation is to consider the output to be comprised of a series of peaks, and in the region near a maximum, the intensity profile

$$Q \cong Q_p e^{-\sigma_\omega^2 (t - t_p)^2}, \tag{2.15}$$

where Q_p is the maximum intensity of the peak centered about $t = t_p$. This suggests that we can approximate the (average) rms width of the temporal spike by [15]

$$\langle \delta t \rangle \cong \frac{1}{\sqrt{2}\sigma_\omega}. \tag{2.16}$$

The average spacing between the spikes [see Eq. (2.27)] is given by [13,15]

$$\langle \Delta t \rangle \cong \frac{\sqrt{2\pi}}{\sigma_\omega}. \tag{2.17}$$

Let us consider the scaled field amplitude

$$a(t) = A(t)/\sqrt{\langle |A|^2 \rangle}. \tag{2.18}$$

Equations (2.18) and (1.3) demonstrate that $a(t)$ is the sum of independent random variables, so its statistical properties are determined by the central limit theorem. Together with the expression for the correlation given in Eq. (2.10), this implies that $a(t)$ is a stationary Gaussian random process, whose correlations are given by $\langle a(t) \rangle = 0$,

$$\langle a(t_1) a(t_2) \rangle = 0, \tag{2.19}$$

$$\langle a(t_1) a^*(t_2) \rangle = \exp\left(-\frac{\sigma_\omega^2 (t_1 - t_2)^2}{2} \right), \tag{2.20}$$

$$\langle |a(t_1)|^2 |a(t_2)|^2 \rangle = 1 + |\langle a(t_1) a^*(t_2) \rangle|^2. \tag{2.21}$$

One can also write

$$\langle a(t_1) a^*(t_2) \rangle = \int d\Omega \, w(\Omega) e^{-i\Omega(t_1 - t_2)}, \tag{2.22}$$

where the spectral weight $w(\Omega)$ is given by

$$w(\Omega) = \frac{1}{\sqrt{2\pi}\sigma_\omega} \exp\left(-\frac{\Omega^2}{2\sigma_\omega^2} \right). \tag{2.23}$$

Introducing the amplitude $R(t)$ and phase $\phi(t)$ via

$$a(t) = R(t)e^{i\phi(t)}, \tag{2.24}$$

we define the normalized variables

$$\rho = \frac{R}{\sqrt{2}}, \quad \eta = \frac{-R''}{\sigma_\omega^2\sqrt{2}}, \quad \nu = \frac{\phi'}{\sigma_\omega}, \quad \mu = \frac{\phi''}{\sigma_\omega^2}. \tag{2.25}$$

Rice [13] has shown (see the Appendix) that the probability $p(\rho,\eta,\nu,\mu)d\rho\, d\eta\, d\nu\, d\mu\, dt$ of finding an extremum of intensity in the interval $d\rho\, d\eta\, d\nu\, d\mu\, dt$ is given by

$$p(\rho,\eta,\nu,\mu) = \frac{8\sigma_\omega}{\pi^2}|\eta|\rho^3 \exp[-3\rho^2 + 2\eta\rho - (\eta+\nu^2\rho)^2 - \rho^2\mu^2]. \tag{2.26}$$

Maxima correspond to $\eta > 0$ and minima to $\eta < 0$.

This distribution was first derived by Rice [13] 60 years ago, as part of a study of the stability of repeaters in a loaded telephone transmission line. The envelope R was associated with the "returned current" produced by reflections from line irregularities. It also applies [15] to the description of the chaotic SASE optical field. This is a beautiful example of how mathematics can unify the description of very different physical problems. The FROG measurements of SASE output reported in Refs. [16,17] provide an experimental laboratory for the study of the statistical theory of shot noise random processes as developed by Rice. In the applications Rice had in mind, he was only interested in the behavior of the envelope R. Consideration of the time evolution of the SASE chaotic radiation field stimulates our interest in the behavior of the phase ϕ.

The number of spikes per unit time [13], N_t, is found by integrating the distribution of Eq. (2.26),

$$N_t = \frac{1}{\langle \Delta t\rangle} = \int_0^\infty d\rho \int_0^\infty d\eta \int_{-\infty}^\infty d\nu \int_{-\infty}^\infty d\mu\, p(\rho,\eta,\nu,\mu)$$
$$= \frac{\sigma_\omega}{3^{5/4}\sqrt{2\pi}} \sum_{n=0}^\infty \frac{(n+1)\Gamma\left(\frac{n}{2}+\frac{5}{4}\right)}{3^{n/2}\Gamma\left(\frac{n}{2}+\frac{7}{4}\right)} \cong \frac{\sigma_\omega}{\sqrt{2\pi}}. \tag{2.27}$$

One can also derive [13] the probability $[dp(\rho)/d\rho]d\rho$ of finding a maximum in the interval $d\rho$,

$$\frac{dp(\rho)}{d\rho} = \frac{1}{N_t}\int_0^\infty d\eta \int_{-\infty}^\infty d\nu \int_{-\infty}^\infty d\mu\, p(\rho,\eta,\nu,\mu)$$
$$= \left(\frac{2}{\pi}\right)^{1/2} \frac{\sigma_\omega}{N_t}\rho^{3/2}e^{-3\rho^2} \sum_{n=0}^\infty \frac{(n+1)\rho^n}{\Gamma\left(\frac{n}{2}+\frac{7}{4}\right)}. \tag{2.28}$$

In Ref. [15], we discussed the probability distribution $dp(Q_{\max})/dQ_{\max} = (d\rho/dQ_{\max})[dp(\rho)/d\rho]_{\rho=\sqrt{Q_{\max}/2}}$ of finding a spike with maximum normalized intensity $Q_{\max} = R^2 = 2\rho^2$ (Fig. 3). In principle one can measure the distribution of intensity at the peak of SASE spikes, but in the experiment of Refs. [16,17] this was not possible because of normalization issues.

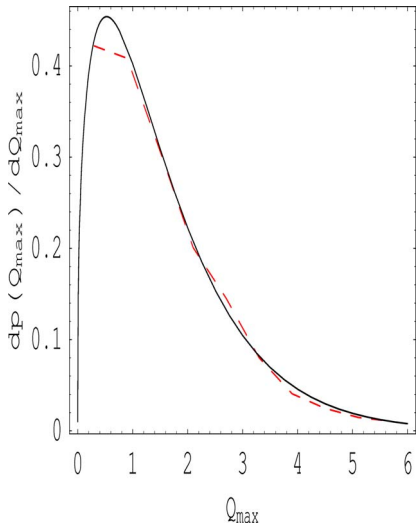

FIG. 3. (Color online) The distribution of normalized peak intensity $dp(Q_{\max})/dQ_{\max}$ as derived from Eq. (2.28) (solid curve) and as obtained from simulation (dashed curve).

The simulation results shown in Figs. 3–6 are carried out using Eq. (1.3) with 200 electron bunches each containing 5000 electrons uniformly distributed on the interval $0 \leqslant t_j \leqslant 1$. The rms wave packet width $\sigma = 0.014$, the radiation frequency $f_r = \omega_r/2\pi = 500.1$, the coherence time $T_{\text{coh}} = 0.043$, the mode number $M = 23$, and the average number of spikes per unit time, $N_t = 16$.

The distribution of R/R'' is closely related to the distribution of rms spike width δt. Let us introduce the variable $s \equiv |\eta|/\rho = |R''|/(R\sigma_\omega^2)$. Suppose the spikes have a Gaussian profile, $R(t) = R_p \exp[-t^2/4(\delta t)^2]$. At the peak $t = 0$ of a Gaussian, we see that $s = 1/(\sqrt{2}\sigma_\omega \delta t)^2$, i.e., the variable s is a measure of the square of the inverse rms width. To proceed, we express the distribution of Eq. (2.26) in terms of the variable s (upper signs apply for intensity maxima and lower for intensity minima):

$$\hat{p}(\rho,s,\nu,\mu) = \frac{8\sigma_\omega}{\pi^2} s\rho^5 \exp\{-\rho^2[3 \mp 2s + (s \pm \nu^2)^2 + \mu^2]\}. \tag{2.29}$$

This follows from $\hat{p}(\rho,s,\nu,\mu)d\rho\, ds\, d\nu\, d\mu = p(\rho,\eta,\nu,\mu)d\rho\, d\eta\, d\nu\, d\mu$. The distribution of the square of the inverse widths at the maxima is (see Fig. 4),

$$\frac{dp(s)}{ds} = \frac{1}{N_t}\int_{-\infty}^\infty d\nu \int_{-\infty}^\infty d\mu \int_0^\infty d\rho\, \hat{p}(\rho,s,\nu,\mu)$$
$$= \frac{6\sigma_\omega}{\pi N_t}\int_0^\infty \frac{s\, d\nu}{[3 - 2s + (s+\nu^2)^2]^{5/2}}. \tag{2.30}$$

From an experimental point of view, it is more natural to consider the distribution of the normalized width $w = 1/\sqrt{s} = \sqrt{2}\sigma_\omega \delta t$, which is determined by $dp/dw = |ds/dw|[dp/ds]_{s=1/w^2}$.

The average normalized width of a spike is

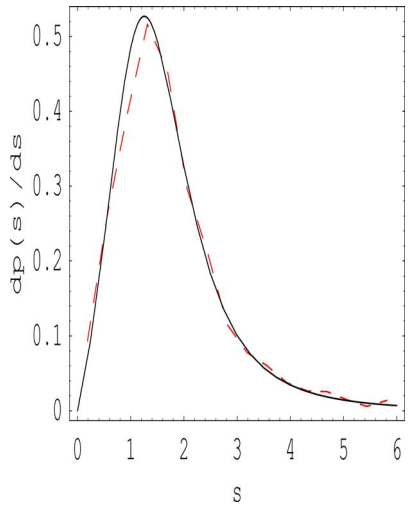

FIG. 4. (Color online) The distribution $dp(s)/ds$ as given in Eq. (2.30) (solid curve) and by simulation (dashed curve). Recall that $s \equiv \eta/\rho = |R''|/(R\sigma_\omega^2)$ is a measure of the square of the inverse rms spike width.

$$\langle w \rangle = \int_0^\infty dw\, w p(w) = 0.87, \tag{2.31}$$

so

$$\langle \delta t \rangle = \frac{0.87}{\sqrt{2}\sigma_\omega}. \tag{2.32}$$

Assuming that the spikes have Gaussian shape [15], $\langle \delta t \rangle$ is the average rms temporal width of the intensity maxima. Note that Eq. (2.32) is in good agreement with the approximation given in Eq. (2.16).

In Refs. [16,17], to make a comparison with the experimental data, it was useful to consider the distribution of the normalized width $\xi = w/\langle w \rangle$:

$$\frac{dp(\xi)}{d\xi} = \frac{6\sigma_\omega}{\pi N_t} \frac{\langle w \rangle}{(\langle w \rangle \xi)^5} \times \int_0^\infty \frac{d\nu}{\{3 - 2/(\langle w \rangle \xi)^2 + [1/(\langle w \rangle \xi)^2 + \nu^2]^2\}^{5/2}}. \tag{2.33}$$

Our analytic calculations are based on the assumption of an electron bunch length long compared to the coherence length. In the experiment, the electron bunch length was comparable to the coherence length. Consideration of the distribution of the normalized width ξ helped to take into account this difference and good agreement between experiment and theory was found. See Sec. IV.

From Eq. (2.26), we can also determine the distributions (Fig. 5) of the normalized frequency deviation from resonance, $\nu = \phi'/\sigma_\omega$ at both intensity maxima (+) and minima (−):

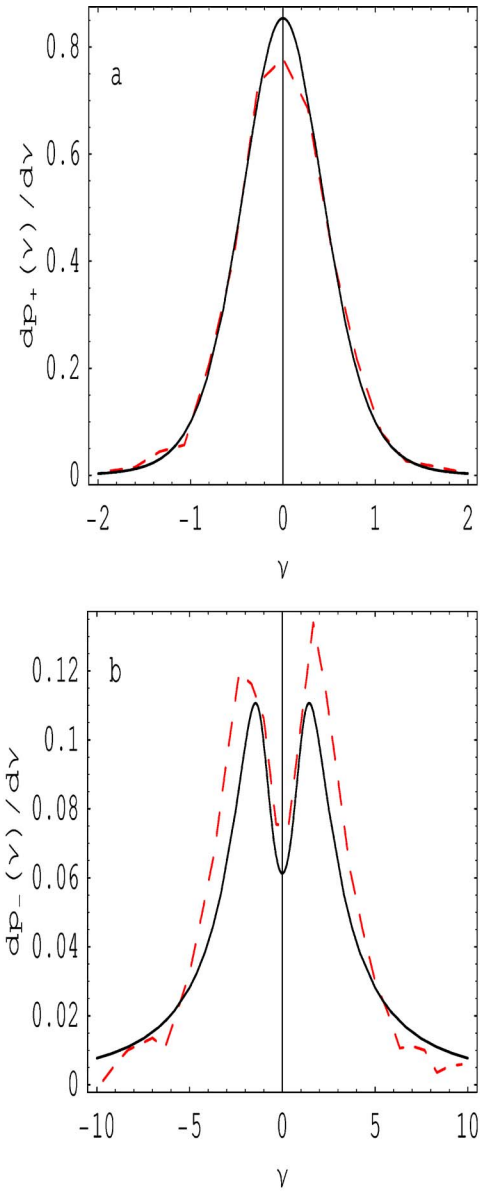

FIG. 5. (Color online) The distributions of normalized frequency deviation $\nu = \phi'/\sigma_\omega$ at (a) intensity maxima and (b) intensity minima as given by Eq. (2.34) (solid curve) and by simulation (dashed curve).

$$\frac{dp_\pm(\nu)}{d\nu} = \frac{1}{N_t} \int_0^\infty ds \int_{-\infty}^\infty d\mu \int_{-\infty}^\infty d\rho\, \hat{p}(\rho, s, \nu, \mu) = \frac{\sigma_\omega}{\pi N_t} \frac{1}{\sqrt{3 + \nu^4}[\sqrt{3 + \nu^4} \pm (\nu^2 - 1)]^2}. \tag{2.34}$$

We note that the frequency deviation from the resonant value is much smaller at the intensity maxima than at the minima. The larger frequency deviation at the minima corresponds to the rapid phase variation related to the loss of coherence between spikes. The frequency distributions presented in Fig. 5 were found [16,17] to be in agreement with experimental FROG measurements as discussed in Sec. IV.

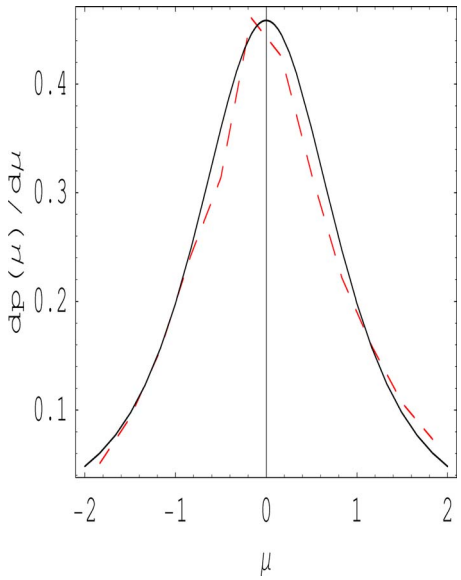

FIG. 6. (Color online) Distribution of normalized frequency chirp $\mu=\phi''/\sigma_\omega^2$ at intensity maxima as given by Eq. (2.35) (solid curve) and by simulation (dashed curve).

The distributions (Fig. 6) describing the frequency chirp $\mu=\phi''/\sigma_\omega$ at intensity maxima (+) and minima (−), are also found from Eq. (2.26):

$$\frac{dp_\pm(\mu)}{d\mu}=\frac{1}{N_t}\int_{-\infty}^{\infty}d\nu\int_0^\infty ds\int_0^\infty d\rho\,\hat{p}(\rho,s,\nu,\mu)$$
$$=\frac{8\sigma_\omega}{\pi^2N_t}\int_{-\infty}^{\infty}d\nu\,f(1,\pm(\nu^2-1),3+\nu^4+\mu^2), \tag{2.35}$$

where

$$f(a,b,c)=\int_0^\infty\frac{x\,dx}{(ax^2+bx+c)^3}=\frac{1}{4c\Delta}+\frac{3b^2}{8c\Delta^2}$$
$$+\frac{3ab}{8\Delta^{5/2}}\left[\arctan\left(\frac{b}{\sqrt{\Delta}}\right)-\frac{\pi}{2}\right] \tag{2.36}$$

and $\Delta=ac-b^2$. In the case of spikes in a bunch long compared to coherence time, the distribution $p(\mu)$ is symmetric about $\mu=0$, with the most likely value being zero chirp. This is different from the situation for a bunch with length similar to the coherence length, for which the distribution is peaked about a nonvanishing value of the chirp [19].

III. STATISTICAL TREATMENT FOR GAUSSIAN ELECTRON BUNCH DENSITY

Let us now discuss the extension of Rice's analysis to a Gaussian bunch density. A full treatment of SASE from a Gaussian bunch would take into account the dependence of the FEL gain on the electron density profile, which results in a dependence of the wave packet duration σ [Eq. (1.3)] on the temporal position in the pulse. In our discussion, we shall ignore this dependence and consider constant σ.

We suppose the electron bunch to have a Gaussian average density profile

$$w_b(t)=\frac{1}{\sqrt{2\pi}\sigma_b}\exp\left(-\frac{t^2}{2\sigma_b^2}\right), \tag{3.1}$$

and consider the time dependence of the SASE amplitude (1.3) observed at a fixed position z. Suppressing the dependence on z, we write the complex, slowly varying amplitude in the form

$$A(t)=A_0\sum_{j=1}^{Ne}\exp\left(\frac{-\chi(t-t_j)^2}{4\sigma^2}+i\omega_r t_j\right), \tag{3.2}$$

where $\chi=1+i\kappa$ with $\kappa=1/\sqrt{3}$. The arrival time t_j of the jth electron at the undulator entrance is randomly distributed according to the Gaussian distribution $w_b(t)$ of Eq. (3.1). Averaging over the stochastic ensemble of arrival times, we determine the field correlation function

$$\langle A(t_1)A^*(t_2)\rangle=\frac{N_e\sigma A_0^2}{\sqrt{\sigma_b^2+\sigma^2}}\exp\left(\frac{-(1+\kappa^2)\sigma_b^2(t_1-t_2)^2-2\sigma^2(\chi t_1^2+\chi^* t_2^2)}{8(\sigma_b^2+\sigma^2)\sigma^2}\right). \tag{3.3}$$

In deriving Eq. (3.3), we have retained only the dominant contributions characterized by the absence of rapid phase variation. These correspond to keeping pairwise equal summation indices from the A and A^* terms. It is also easily seen that the average of the field vanishes, $\langle A(t)\rangle=0$.

The Wigner function [20] is defined by

$$W(t,\omega)=\int d\tau\left\langle A\left(t-\frac{\tau}{2}\right)A^*\left(t+\frac{\tau}{2}\right)\right\rangle\exp[-i(\omega-\omega_r)\tau]. \tag{3.4}$$

From Eqs. (3.3) and (3.4), we derive

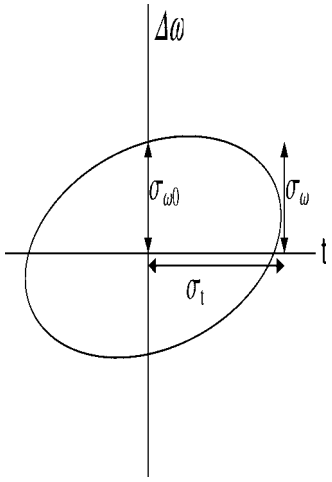

FIG. 7. Region of phase space occupied by radiation. $\Delta\omega=\omega-\omega_r$. Area is $2\pi\sigma_t\sigma_{\omega 0}$.

$$W(t,\omega)=\frac{N_e\sigma A_0^2\sqrt{2\pi}}{\sigma_t\sigma_{\omega 0}}\exp\left(-\frac{t^2}{2\sigma_t^2}-\frac{(\omega-\omega_r-ut)^2}{2\sigma_{\omega 0}^2}\right), \tag{3.5}$$

where

$$\sigma_t^2=\sigma_b^2+\sigma^2,\quad \sigma_{\omega 0}^2=\frac{1+\kappa^2}{4\sigma^2}-\frac{\kappa^2}{4\sigma_t^2},\quad u=\frac{\kappa}{2\sigma_t^2}. \tag{3.6}$$

Note that for a long pulse, the chirp u [Eq. (3.6)] vanishes inversely proportionally to the square of the pulse duration.

Integrating the Wigner function over frequency we obtain the average instantaneous intensity,

$$\langle|A(t)|^2\rangle=\int\frac{d\omega}{2\pi}W(t,\omega)=\frac{N_e\sigma A_0^2}{\sigma_t}\exp\left(-\frac{t^2}{2\sigma_t^2}\right), \tag{3.7}$$

and integrating over time, the average spectral intensity

$$\langle|\tilde{A}(\omega)|^2\rangle=\int dt\, W(t,\omega)=\frac{2\pi N_e\sigma A_0^2}{\sigma_\omega}\exp\left(-\frac{(\omega-\omega_r)^2}{2\sigma_\omega^2}\right). \tag{3.8}$$

It is seen that the rms radiation bandwidth is given by

$$\sigma_\omega^2=\sigma_{\omega 0}^2+u^2\sigma_t^2=\frac{1+\kappa^2}{4\sigma^2}. \tag{3.9}$$

The phase space area occupied by the SASE radiation (see Fig. 7) is proportional to the product $\sigma_t\sigma_{\omega 0}$. The uncertainty principle sets a lower bound of $\frac{1}{2}$ for the quantity $\sigma_t\sigma_{\omega 0}$. The ratio of $\sigma_t\sigma_{\omega 0}$ to the minimum value is given by

$$2\sigma_t\sigma_{\omega 0}=\sqrt{1+\frac{(1+\kappa^2)\sigma_b^2}{\sigma^2}}. \tag{3.10}$$

This ratio is expected to be equal to the number of modes. Support for this is presented in the following.

Let us introduce the scaled field amplitude $\alpha(t)$ via

$$A(t)=A_0\sqrt{\frac{N_e\sigma}{\sigma_t}}\exp\left(-\frac{\chi t^2}{4\sigma_t^2}\right)\alpha(t). \tag{3.11}$$

It now follows from Eq. (3.3) that the correlation of the scaled field is

$$g_1(t_1-t_2)\equiv\langle\alpha(t_1)\alpha^*(t_2)\rangle=\exp\left(-\frac{\sigma_\alpha^2}{2}(t_1-t_2)^2\right), \tag{3.12}$$

where we define

$$\sigma_\alpha^2=\sigma_{\omega 0}^2-\frac{1}{4\sigma_t^2}. \tag{3.13}$$

We can also write

$$\langle\alpha(t_1)\alpha^*(t_2)\rangle=\int d\Omega\, w_\alpha(\Omega)e^{-i\Omega(t_1-t_2)}, \tag{3.14}$$

where the spectral weight $w_\alpha(\Omega)$ is given by

$$w_\alpha(\Omega)=\frac{1}{\sqrt{2\pi}\sigma_\alpha}\exp\left(-\frac{\Omega^2}{2\sigma_\alpha^2}\right). \tag{3.15}$$

The total radiation bandwidth σ_ω is related to σ_α by

$$\sigma_\omega^2=\sigma_\alpha^2+\frac{1+\kappa^2}{4\sigma_t^2}=\frac{1+\kappa^2}{4\sigma^2} \tag{3.16a}$$

and

$$\frac{\sigma_b}{\sigma_t}=\frac{\sigma_\alpha}{\sigma_\omega}. \tag{3.16b}$$

The coherence time [21] is defined by

$$T_{\rm coh}\equiv\int d\tau\left|\frac{\left\langle A\left(t-\frac{\tau}{2}\right)A^*\left(t+\frac{\tau}{2}\right)\right\rangle}{\langle|A(t)|^2\rangle}\right|^2. \tag{3.17}$$

Using Eqs. (3.11)–(3.13), we find

$$T_{\rm coh}=\frac{\sqrt{\pi}}{\sigma_{\omega 0}}. \tag{3.18}$$

Let us now introduce

$$g_2(t_1-t_2)\equiv\langle|\alpha(t_1)|^2|\alpha(t_2)|^2\rangle=1+|g_1(t_1-t_2)|^2. \tag{3.19}$$

The fluctuation σ_W of the energy W in a pulse can be expressed in the form

$$\frac{\sigma_W^2}{W^2}=\frac{\int dt_1dt_2[\langle|A(t_1)|^2|A(t_2)|^2\rangle-\langle|A(t_1)|^2\rangle\langle|A(t_2)|^2\rangle]}{\int dt_1\langle|A(t_1)|^2\rangle\int dt_2\langle|A(t_2)|^2\rangle}. \tag{3.20}$$

Using Eqs. (3.11) and (3.19), this can be rewritten as

$$\frac{\sigma_W^2}{W^2} = \int \frac{dt_1 dt_2}{2\pi\sigma_t^2} \exp\left(\frac{-t_1^2 - t_2^2}{2\sigma_t^2}\right) |g_1(t_1 - t_2)|^2. \quad (3.21)$$

Following Ref. [8], we define the number of modes M by

$$\frac{\sigma_W^2}{W^2} = \frac{1}{M}. \quad (3.22)$$

Equations (3.12) and (3.21) imply that

$$M = \sqrt{1 + 4\sigma_\alpha^2 \sigma_t^2}. \quad (3.23)$$

From Eqs. (3.10), (3.13), and (3.18), it is seen that this implies

$$M = 2\sigma_t \sigma_{\omega 0} = \frac{2\sqrt{\pi}\sigma_t}{T_{\text{coh}}}. \quad (3.24)$$

Hence, we have shown that the number of modes as defined in terms of the energy fluctuation [Eq. (3.22)] is equal to the number of minimum area phase space cells occupied by the radiation.

One can also express the number of modes M in terms of the Wigner function via

$$\frac{\int dt\, d\omega\, W^2(t,\omega)}{\left(\int dt\, d\omega\, W(t,\omega)\right)^2} = \frac{\int dt_1 dt_2 |\langle A(t_1) A^*(t_2)\rangle|^2}{W^2} = \frac{1}{M}. \quad (3.25)$$

The quantity on the left-hand side is often used as a measure of the total degree of coherence [20]. For Gaussian random fields,

$$|\langle A(t_1) A^*(t_2)\rangle|^2 = \langle |A(t_1)|^2 |A(t_2)|^2\rangle - \langle |A(t_1)|^2\rangle \langle |A(t_2)|^2\rangle, \quad (3.26)$$

and Eq. (3.25) is equivalent to the definition given in Eq. (3.22). For more general fields, where Eq. (3.26) does not hold, Eq. (3.25) may provide a better definition of the number of modes. In particular, for a fully coherent field with no energy fluctuation, Eq. (3.25) still holds and says there is one mode.

Let us introduce the Fourier transform of the field,

$$\tilde{A}(\Omega) = \int dt\, e^{i\Omega t} A(t). \quad (3.27)$$

Inserting Eq. (3.2) for $A(t)$, we find

$$\tilde{A}(\Omega) = A_0 \sqrt{N_e \frac{4\pi\sigma^2}{\chi}} \exp\left(-\frac{\sigma^2\Omega^2}{\chi}\right) \tilde{b}(\Omega), \quad (3.28)$$

where

$$\tilde{b}(\Omega) = \frac{1}{\sqrt{N_e}} \sum_{j=1}^{N_e} e^{i(\omega_r + \Omega) t_j}. \quad (3.29)$$

$\tilde{b}(\Omega)$ is the normalized Fourier transform of the incident electron density $b(t) = \sum_{j=1}^{N_e} \delta(t - t_j)$. Since $\tilde{b}(\Omega)$ is a sum of independent random terms, its statistical behavior is described by the central limit theorem [13]. It is easily seen that $\langle \tilde{b}(\Omega)\rangle = 0$ and

$$\langle \tilde{b}(\Omega_1) \tilde{b}^*(\Omega_2)\rangle = \exp\left(-\frac{\sigma_b^2}{2}(\Omega_1 - \Omega_2)^2\right). \quad (3.30)$$

We can also write

$$\langle \tilde{b}(\Omega_1) \tilde{b}^*(\Omega_2)\rangle = \int dt\, w_b(t) e^{-it(\Omega_1 - \Omega_2)}, \quad (3.31)$$

where the temporal electron density $w_b(t)$ was introduced in Eq. (3.1).

The range of spectral coherence [21] is defined by

$$\Omega_{\text{coh}} = \int d\Omega' \left| \frac{\left\langle \tilde{A}\left(\Omega - \frac{\Omega'}{2}\right) \tilde{A}^*\left(\Omega + \frac{\Omega'}{2}\right)\right\rangle}{\langle |\tilde{A}(\Omega)|^2\rangle} \right|^2. \quad (3.32)$$

Using Eqs. (3.28), (3.30), and (3.32), we find that

$$\Omega_{\text{coh}} = \sqrt{\frac{\pi}{\sigma_b^2 + \frac{1}{4\sigma_\omega^2}}}. \quad (3.33)$$

Since, $\sigma_t^2 \sigma_{\omega 0}^2 = \sigma_b^2 \sigma_\omega^2 + 1/4$, it follows that the number of modes can also be expressed in the form

$$M = 2\sigma_t \sigma_{\omega 0} = \frac{2\sqrt{\pi}\sigma_\omega}{\Omega_{\text{coh}}}. \quad (3.34)$$

In summary, Eqs. (3.2) and (3.11) demonstrate that the scaled field $\alpha(t)$ is the sum of independent random variables, so its statistical properties are determined by the central limit theorem. Together with the expression for the correlation given in Eq. (3.12), this implies that $\alpha(t)$ is a stationary Gaussian random process. Therefore, all the analysis [13] discussed in Sec. II for a uniform electron distribution applies to the statistics of the scaled field $\alpha(t)$ for a Gaussian electron density. Using Eq. (3.11), this in turn determines the statistical properties of the actual field amplitude $A(t)$ emitted by a Gaussian bunch. We have shown that $\langle \alpha(t)\rangle = 0$, $\langle \alpha(t_1)\alpha(t_2)\rangle = 0$,

$$\langle \alpha(t_1) \alpha^*(t_2)\rangle = \exp\left(-\frac{\sigma_\alpha^2 (t_1 - t_2)^2}{2}\right), \quad (3.35)$$

$$\langle |\alpha(t_1)|^2 |\alpha(t_2)|^2\rangle = 1 + |\langle \alpha(t_1) \alpha^*(t_2)\rangle|^2. \quad (3.36)$$

It is useful to write

$$\langle \alpha(t_1) \alpha^*(t_2)\rangle = \int d\Omega\, w_\alpha(\Omega) e^{-i\Omega(t_1 - t_2)}, \quad (3.37)$$

where the spectral weight $w(\Omega)$ is given by

$$w_\alpha(\Omega) = \frac{1}{\sqrt{2\pi}\sigma_\alpha} \exp\left(-\frac{\Omega^2}{2\sigma_\alpha^2}\right), \quad (3.38)$$

and σ_α was defined in Eq. (3.13). The total radiation bandwidth σ_ω is related to σ_α by

$$\sigma_\omega^2 = \sigma_\alpha^2 + \frac{1+\kappa^2}{4\sigma_t^2} = \frac{1+\kappa^2}{4\sigma^2}. \tag{3.39}$$

Recall, that σ is the SASE wave packet duration introduced in Eq. (3.2), and $\kappa = 1/\sqrt{3}$.

Results in the frequency domain are obtained by making the replacements:

$$\alpha(t) \to \tilde{b}(\Omega), \tag{3.40a}$$

$$w_\alpha(\Omega) \to w_b(t), \tag{3.40b}$$

$$\sigma_\alpha \to \sigma_b. \tag{3.40c}$$

In this section, we have ignored the effect of the dependence of gain on the local electron density. It is our belief that when one includes the effect of the density dependence of the gain, the relation given in Eq. (3.6) between the radiation pulse duration σ_t and the electron bunch duration σ_b is modified, but to good approximation the statistical behavior as described in this section is correct.

In the case when the coherence time is small compared to the electron bunch distribution ($\sigma \ll \sigma_b$), the results simplify and can be summarized as follows:

$$M \cong 2\sigma_t\sigma_\omega \quad \text{(number of modes)}, \tag{3.41}$$

$$\langle \Delta t \rangle \cong \frac{\sqrt{2\pi}}{\sigma_\omega} \quad \text{(average temporal spike separation)}, \tag{3.42}$$

$$\langle \delta t \rangle \cong \frac{1}{\sqrt{2}\sigma_\omega} \quad \text{(average temporal spike width)}, \tag{3.43}$$

$$T_{coh} \cong \frac{\sqrt{\pi}}{\sigma_\omega} \quad \text{(coherence time)}, \tag{3.44}$$

$$M \cong \frac{2\sqrt{\pi}\sigma_t}{T_{\rm coh}}, \tag{3.45}$$

$$\langle \Delta\omega \rangle \cong \frac{\sqrt{2\pi}}{\sigma_t} \quad \text{(average frequency spike separation)}, \tag{3.46}$$

$$\langle \delta\omega \rangle \cong \frac{1}{\sqrt{2}\sigma_t} \quad \text{(average frequency spike width)}, \tag{3.47}$$

$$\Omega_{\rm coh} \cong \frac{\sqrt{\pi}}{\sigma_t} \quad \text{(range of frequency coherence)}, \tag{3.48}$$

$$M \cong \frac{2\sqrt{\pi}\sigma_\omega}{\Omega_{\rm coh}}. \tag{3.49}$$

TABLE I. Main experimental parameters.

Peak current	850 A
Effective FWHM bunch length (T_b)	0.9 ps
rms normalized emittance	9π mm mrad
Undulator period (λ_u)	3.3 cm
Undulator length (each section)	2.4 m
Undulator strength parameter (K)	3.1
Beam energy (γmc^2)	217 MeV
Nominal radiation wavelength (λ_r)	530 nm
FWHM SASE bandwidth ($\Delta\lambda$)	~3 nm
Gain length (L_G)	0.68 m

IV. COMPARISON WITH EXPERIMENTAL RESULTS

The experiment was conducted at the Low-Energy Undulator Test Line at the Advanced Photon Source [16,17,19]. A detailed description of the facility was presented earlier [5] and Table I is a summary of the main parameters for the experiment. (FWHM indicates full width at half-maximum).

Briefly, a high-brightness electron bunch generated from a rf photocathode gun is compressed through a magnetic chicane and then accelerated to 217 MeV in energy for operation at 532 nm, a wavelength chosen so a FROG device in the second-harmonic configuration can be used.

The electron beam is sent into an undulator line. Exponential gain and saturation were verified by measuring the FEL energy after each undulator, and a gain length of $L_G = 0.68$ m was obtained.

The output from undulator 5 is directed through a number of collimating optics to a single-shot FROG device using the second-harmonic gating geometry [10]. The FROG device records single-shot spectrograms of the correlation signal of two replicas of the input pulses from a 0.5 mm type-I BBO crystal. For the second-harmonic gating geometry used in this experiment, the autocorrelation field signal is $E_{\rm sig}(t,\tau) \propto E(t)E(t-\tau)$, where τ is the relative delay. When recording the spectrum, the observed trace is the so-called spectrogram $I_{\rm FROG}(\omega,\tau) \propto \left|\int_{-\infty}^{\infty} E_{\rm sig}(t,\tau)\exp(-i\omega t)dt\right|^2$, and contains the information of both the amplitude and the phase of the input, which is then retrieved using an iterative algorithm. Note that for this FROG geometry there is an ambiguity about the direction of time.

Each FROG image and its retrieval show a full characterization of the pulse, including the field amplitude and the phase. This is an advantage over the traditional time-integrated experiments such as the intensity interferometer. In addition, study of the shot-to-shot variation of multiple pulses provides information on the statistics of the chaotic optical field.

Let us first consider the time-domain intensity spikes [16]. In Figs. 8(a) and 8(b), we show the probability distributions of the normalized rms spike width $\xi = \delta t/\langle \delta t \rangle$ and the normalized spacing between the intensity maxima $\zeta = \Delta t/\langle \delta t \rangle$. For the ensemble of the pulses we measured, $\langle \delta t \rangle = 52$ fs is the average value of the rms spike width. In Fig. 8(a), the distribution of the spike width peaks at a value slightly smaller

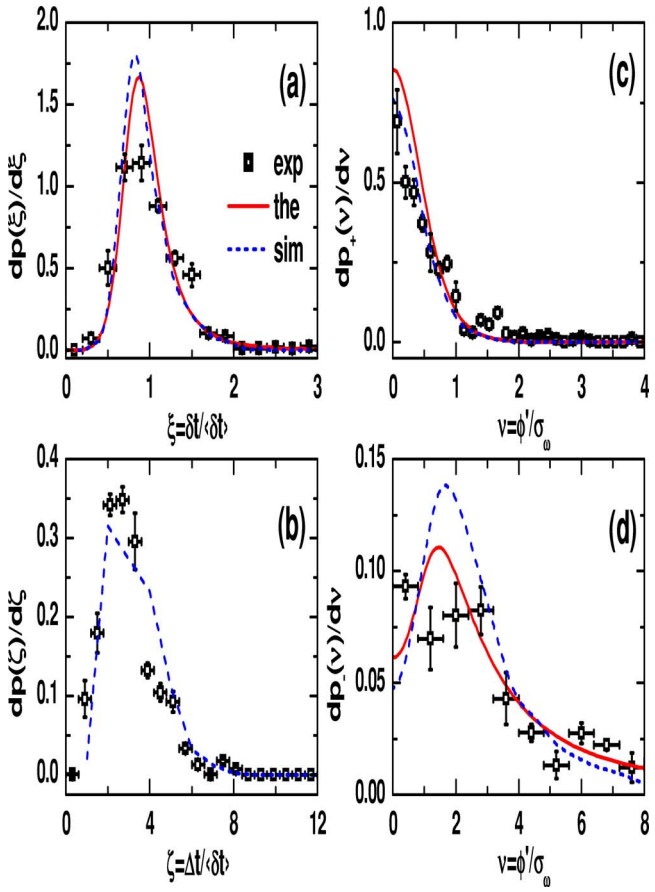

FIG. 8. (Color online) Time-domain statistics measurement. Distribution of (a) the spike width δt and (b) the peak-to-peak spacing Δt between the intensity spikes normalized to the average spike width $\langle \delta t \rangle$. Phase derivative at the intensity maxima (c) and minima (d) normalized to the rms SASE FEL bandwidth. Experimental data (symbols), theoretical calculation (solid line), and simulation results (dashed lines) are all presented when possible. Note the different horizontal scales for (c) and (d).

than the average. It has a long tail extending to larger spike width and an abrupt drop at smaller spike width. The distribution in Fig. 8(b) for the spike spacing peaks at about $\zeta = 3.0$, and its average is 3.25, in reasonable agreement with the theoretical expectation $\langle \Delta t \rangle / \langle \delta t \rangle = 2\sqrt{\pi} \cong 3.5$ [see Eqs. (3.42) and (3.43)] for a totally chaotic optical field. Also shown in Figs. 8(a) and 8(b) are the results of the numerical simulation (dashed lines).

The experimental result for the distribution of rms widths compares favorably with the analytic result derived in Eq. (2.33)

$$\frac{dp(\xi)}{d\xi} = \frac{ab}{(a\xi)^5} \int_0^\infty \frac{d\nu}{\{3 - 2/(a\xi)^2 + [1/(a\xi)^2 + \nu^2]^2\}^{5/2}}, \tag{4.1}$$

where $\xi = \delta t / \langle \delta t \rangle$, $a \cong 0.8685$, and $b \cong 9.510$, shown in solid line in Fig. 8(a). This distribution is normalized and its average value is unity. As noted in Sec. II, for the analytical theory the rms width of an intensity spike has been approximated by $\sqrt{-I/I''}$, where the intensity I and its second time derivative I'' are evaluated at the intensity maximum. For the experimental data and simulation, the rms width is estimated by measuring the full width at half maximum of those spikes with measurable FWHM and dividing by 2.35. In all cases, the spikes are assumed to have a Gaussian shape. Note the analytical calculation assumes an infinitely long pulse.

Intuitively, since an individual intensity spike corresponds to a coherent region, the phase within the spike is expected to be correlated. On the other hand, due to the lack of communication between different coherence regions, there can be a phase jump in the transition region between two spikes, as illustrated in Fig. 1. We quantified this phase behavior by measuring the time derivative of the phase (ϕ') of the slowly varying envelope at the intensity maxima and minima. The measured distributions (symbols) are presented in Figs. 8(c) and 8(d), which show that indeed the phase drift rate is small at the intensity maxima but may be much larger at the intensity minima. Also in Figs. 8(c) and 8(d) are the results of simulation (dashed lines). Both simulation and the experiment data are seen to be in good agreement with the theoretical distribution (shown in solid lines) derived in Eq. (2.34),

$$\frac{dp_\pm(\nu)}{d\nu} = \frac{d}{\sqrt{3 + \nu^4}[\sqrt{3 + \nu^4} \pm (\nu^2 - 1)]^2}, \tag{4.2}$$

where $\nu = \phi' / \sigma_\omega$, $d \cong 0.7925$ is a normalizing factor, and p_+ and p_- are the distributions at the intensity maxima and minima, respectively. Note that the distribution of phase drift rate is symmetric with respect to zero (Fig. 5). We only show the positive half of the distribution. Of interest is the observed off-zero maximum of the distribution for the phase drift at the intensity minima, which implies there is a most probable decoherence rate between the coherence regions.

It is of interest to compare the approximate relations given in Eqs. (3.41)–(3.49) with experimental measurements in the time and frequency domains [17]. This is done in Table II, which displays both the experimentally measured value and the value calculated from its reciprocal counterpart ($t \leftrightarrow \omega$) for the rms spike width, spike separation, and coherence range. The agreement is in general excellent. It is seen that the simple relations developed in Sec. III (valid for a long pulse with many coherence regions) do provide a satisfactory first approximation to the experimental behavior. We note that for a short temporal pulse containing only a few spikes, measuring the average spike width $\langle \delta\omega \rangle$ yielded a better estimate of the pulse duration $\bar{\sigma}_t$ than did the measurement of the average spike separation $\langle \Delta\omega \rangle$.

V. CONCLUDING REMARKS

The SASE FEL is a filtered chaotic light source, possessing high intensity and relatively long coherence length. In previous work [22,23], it has been established that the SASE pulse energy is described by the Γ distribution [13,14]. This type of measurement is an example of the conventional photon counting statistics. The time- and frequency-domain results of Refs. [16,17] present a new class of experimental data on the behavior of the SASE chaotic optical field. The

TABLE II. Correlation numbers between time and frequency domains.

		Measured	Calculated
rms width	Time $\bar{\sigma}_t$ (fs)	112	
	Frequency $\bar{\sigma}_\omega$ (mrad/fs)	12	
rms spike width	Time $\langle \delta t \rangle$ (fs)	52	$\langle \delta t \rangle = 1/\sqrt{2}\bar{\sigma}_\omega = 58$ Eq. (3.43)
	Frequency $\langle \delta\omega \rangle$ (mrad/fs)	8.9	$\langle \delta\omega \rangle = 1/\sqrt{2}\bar{\sigma}_t = 6.3$ Eq. (3.47)
Average spike spacing	Time $\langle \Delta t \rangle$ (fs)	169	$\langle \Delta t \rangle = \sqrt{2\pi}/\bar{\sigma}_\omega = 208$ Eq. (3.42)
	Frequency $\langle \Delta\omega \rangle$ (mrad/fs)	19	$\langle \Delta\omega \rangle = \sqrt{2\pi}/\bar{\sigma}_t = 22$ Eq. (3.46)
Coherence range	Time T_{coh} (fs)	$T_{\mathrm{coh}} = \sqrt{2\pi}\langle \delta t \rangle = 130$	$T_{\mathrm{coh}} = \sqrt{\pi}/\bar{\sigma}_\omega = 147$ Eq. (3.44)
	Frequency Ω_{coh} (mrad/fs)	$\Omega_{\mathrm{coh}} = \sqrt{2\pi}\langle \delta\omega \rangle = 22$	$\Omega_{\mathrm{coh}} = \sqrt{\pi}/\bar{\sigma}_t = 21$ Eq. (3.48)
Mode no.	M	$M = 2\bar{\sigma}_\omega\bar{\sigma}_t = 2.8$	

analysis of random noise presented in Secs. II and III provides a good initial description of the new experiments. It remains as a challenge for future theoretical work to include the effect of the dependence of gain on the local electron density, and in particular to determine the temporal duration of the output radiation pulse as a function of the electron bunch length.

ACKNOWLEDGMENTS

The authors thank Z. Huang for helpful discussions. S.K. thanks the Stanford Linear Accelerator Center for its hospitality during the course of this work. This work is supported by the U.S. Department of Energy under Contracts No. W-31-109-ENG-38, No. DE-AC02-98CH10886, and No. DE-AC03-76SF00515.

APPENDIX: DERIVATION OF EQ. (2.26)

Here we review Rice's [13] derivation of the probability distribution [Eq. (2.26)] for intensity extrema. Consider the stochastic function,

$$y = F(\tau_1, \tau_2, \ldots, \tau_N; t) \tag{A1}$$

and its derivative

$$y' = \frac{\partial F}{\partial t}, \tag{A2}$$

where $\tau_1, \ldots, \tau_N$ are random variables. Let $P(\xi, \eta; t)d\xi\, d\eta$ be the probability of finding y between ξ and $\xi + d\xi$, and y' between η and $\eta + d\eta$ at time t. We first wish to determine the probability that there is a zero of the function F having positive slope somewhere in the interval $t_1 < t < t_1 + dt$. Suppose $y = \xi < 0$ at t_1 and $y = 0$ somewhere in $t_1 < t < t_1 + dt$. If the slope at t_1 is $\eta > 0$, then F passes through zero (see Fig. 9) at $t = t_1 - \xi/\eta$. Hence, we require $t_1 < t_1 - \xi/\eta < t_1 + dt$, i.e., $-\eta\, dt < \xi < 0$. Therefore, the probability that there is a zero of F with positive slope in $t_1 < t < t_1 + dt$ is given by

$$\int_0^\infty d\eta \int_{-\eta dt}^0 d\xi\, P(\xi, \eta; t_1) = dt \int_0^\infty \eta\, d\eta\, P(0, \eta; t_1). \tag{A3}$$

We can now determine the probability $p(y_1)dt\, dy$ that F has a maximum with value between y_1 and $y_1 + dy$ in the time interval $t_1 < t_1 + dt$. At a maximum, the derivative of F is zero and its second derivative is negative. From the result of Eq. (A3), we see that

$$p(y_1; t_1)dt\, dy = -\, dt\, dy \int_{-\infty}^0 \varsigma\, d\varsigma\, P(y_1, 0, \varsigma; t_1), \tag{A4}$$

where $P(\xi, \eta, \varsigma; t_1)$ is the probability density function for the variables, $\xi = F(\tau_1, \ldots, \tau_N; t_1)$, $\eta = (\partial F/\partial t)_{t=t_1}$, and $\varsigma = (\partial^2 F/\partial t^2)_{t=t_1}$.

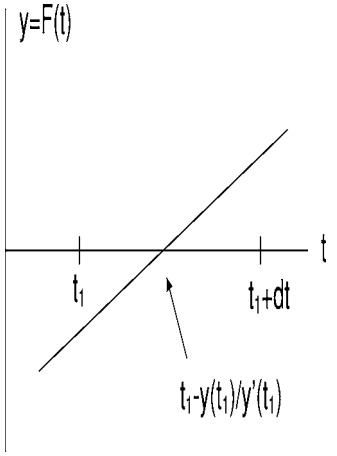

FIG. 9. Illustration of the behavior of a function $y = F(\tau_1, \tau_2, \ldots, \tau_N; t)$ in the neighborhood of a zero with positive slope.

The central limit theorem [13] states that the distribution of the normalized sum of N independent K-component vectors approaches the normal law as $N\to\infty$. In particular, consider the vectors $r_j=(x_{j1},\ldots,x_{jK})\{j=1,\ldots,N\}$ and suppose $\langle r_j\rangle=0$ and $\langle x_{ja}x_{kb}\rangle=0$ for $j\neq k$. Define the vector

$$V=(r_1+\cdots+r_N)/\sqrt{N}. \tag{A5}$$

In the limit $N\to\infty$, the distribution $P(V)$ approaches the normal law:

$$P(V)\to(2\pi)^{-K/2}(\det M)^{-1/2}\exp\left(-\frac{1}{2}V^TM^{-1}V\right), \tag{A6}$$

where M is the matrix of moments,

$$M=\begin{bmatrix}\mu_{11} & \mu_{12}\cdots\mu_{1K}\\ \vdots & \\ \mu_{K1} & \mu_{K2}\cdots\mu_{KK}\end{bmatrix}, \tag{A7}$$

with

$$\mu_{ab}=\langle V_aV_b\rangle=\int d^KV(V_aV_b)P(V). \tag{A8}$$

The radiation amplitude and its first and second time derivatives can be expressed as the sum of independent random terms. Therefore, the central limit theorem determines the distribution describing their statistical behavior. We consider the real and imaginary parts of the scaled amplitude and their derivatives $a=x+iy$, $a'=x'+iy'$, $a''=x''+iy''$, where the prime denotes differentiation with respect to time t. Introducing the notation $a^{(m)}=\partial^m a/\partial t^m$, it follows from Eqs. (2.19) and (2.22) that

$$\langle a^{(m)}(t)a^{(n)}(t)\rangle=0 \tag{A9a}$$

and

$$\langle a^{(m)}(t)a^{(n)*}(t)\rangle=2(-i)^{m-n}b_{m+n}, \tag{A9b}$$

where

$$2b_m=\int_{-\infty}^{\infty}d\Omega\, w(\Omega)\Omega^m. \tag{A10}$$

The normalization is chosen so that $b_0=1/2$. The distribution $P(x,y,x',y',x'',y'')$ is given by Eq. (A6), with the vector $V^T=(x,y',x'',y,x',y'')$ and the matrix M of second moments,

$$M=\begin{bmatrix}b_0 & b_1 & -b_2 & 0 & 0 & 0\\ b_1 & b_2 & -b_3 & 0 & 0 & 0\\ -b_2 & -b_3 & b_4 & 0 & 0 & 0\\ 0 & 0 & 0 & b_0 & -b_1 & -b_2\\ 0 & 0 & 0 & -b_1 & b_2 & b_3\\ 0 & 0 & 0 & -b_2 & b_3 & b_4\end{bmatrix}. \tag{A11}$$

We now introduce the magnitude R and phase ϕ of the scaled amplitude via

$$a(t)=R(t)e^{i\phi(t)}. \tag{A12}$$

It follows that

$$x=R\cos\phi, \tag{A13a}$$

$$x'=R'\cos\phi-R\sin\phi\phi', \tag{A13b}$$

$$x''=R''\cos\phi-2R'\sin\phi\phi'-R\cos\phi\phi'^2-R\sin\phi\phi'', \tag{A13c}$$

$$y=R\sin\phi, \tag{A13d}$$

$$y'=R'\sin\phi+R\cos\phi\phi', \tag{A13e}$$

$$y''=R''\sin\phi+2R'\cos\phi\phi'-R'\sin\phi\phi'^2+R\cos\phi\phi'', \tag{A13f}$$

$$dx\,dx'dx''dy\,dy'dy''=R^3dR\,dR'dR''d\phi\,d\phi'd\phi''. \tag{A13g}$$

The distribution describing the amplitude, the phase, and their time derivatives is determined by

$$\begin{aligned}\hat{P}(R,R',R'',\phi,\phi',\phi'')dR\,dR'dR''d\phi\,d\phi'd\phi''\\ =P(x,y,x',y',x'',y'')dx\,dy\,dx'dy'dx''dy''.\end{aligned} \tag{A14}$$

Recalling the discussion leading to Eq. (A4), we see that the probability of finding an extremum of intensity ($R'=0$) in the interval $dR\,dR''\,d\theta\,d\theta'\,d\theta''\,dt$ is given by

$$|R''|\int_0^{2\pi}d\phi\hat{P}(R,R'=0,R'',\phi,\phi',\phi''). \tag{A15}$$

Introducing the normalized variables

$$\rho=\frac{R}{\sqrt{2}},\quad \eta=\frac{-R''}{\sigma_\omega^2\sqrt{2}},\quad \nu=\frac{\phi'}{\sigma_\omega},\quad \mu=\frac{\phi''}{\sigma_\omega^2}, \tag{A16}$$

it follows that the probability $p(\rho,\eta,\nu,\mu)d\rho\,d\eta\,d\nu\,d\mu\,dt$ for finding an extremum of intensity in the interval $d\rho\,d\eta\,d\nu\,d\mu\,dt$ is given by [13]

$$\begin{aligned}p(\rho,\eta,\nu,\mu)=\frac{8\sigma_\omega}{\pi^2}|\eta|\rho^3\exp[-3\rho^2+2\eta\rho-(\eta+\nu^2\rho)^2\\ -\rho^2\mu^2].\end{aligned} \tag{A17}$$

Maxima correspond to $\eta>0$ and minima to $\eta<0$.

[1] A. M. Kondratenko and E. L. Saldin, Sov. Phys. Dokl. **24**(12), 986 (1979).
[2] R. Bonifacio, C. Pellegrini, and L. M. Narducci, Opt. Commun. **50**, 373 (1984).
[3] SLAC Report No. SLAC-R-521, Stanford Linear Accelerator Center, Stanford, CA, 1998 (unpublished).
[4] DESY Report No. DESY97–048, Deutsches Elektronen-Synchrotron, Hamburg, 1997 (unpublished).
[5] S. V. Milton *et al.*, Science **292**, 1953 (2001).
[6] V. Ayvazyan *et al.*, Phys. Rev. Lett. **88**, 104802 (2002).
[7] A. Tremaine *et al.*, Phys. Rev. Lett. **88**, 204801 (2002).
[8] J. W. Goodman, *Statistical Optics* (John Wiley & Sons, New York, 1985).
[9] R. Hanbury Brown and R. Q. Twiss, Nature (London) **177**, 27 (1956).
[10] R. Trebino *et al.*, Rev. Sci. Instrum. **68**, 3277 (1997).
[11] J. M. Wang and L. H. Yu, Nucl. Instrum. Methods Phys. Res. A **250**, 484 (1986).
[12] K. J. Kim, Nucl. Instrum. Methods Phys. Res. A **250**, 396 (1986).
[13] S. O. Rice, Bell Syst. Tech. J. **24**, 46 (1945). See Section 3.8.
[14] E. L. Saldin, E. A. Schneidmiller, and M. V. Yurkov, *The Physics of Free Electron Lasers* (Springer-Verlag, Berlin, 2000), Chap. 6.
[15] S. Krinsky and R. L. Gluckstern, Phys. Rev. ST Accel. Beams **6**, 050701 (2003).
[16] Y. Li, S. Krinsky, J. Lewellen, K. J. Kim, V. Sajaev, and S. Milton, Phys. Rev. Lett. **91**, 243602 (2003).
[17] Y. Li, S. Krinsky, J. Lewellen, and V. Sajaev, Appl. Phys. **B80**, 31 (2004).
[18] R. Bonifacio, L. De Salvo, P. Pierini, N. Piovella, and C. Pellegrini, Phys. Rev. Lett. **73**, 70 (1994).
[19] Y. Li, J. Lewellen, Z. Huang, V. Sajaev, and S. Milton, Phys. Rev. Lett. **89**, 234801–1 (2002).
[20] M. J. Bastiaans, J. Opt. Soc. Am. A **3**, 1227 (1986).
[21] S. Krinsky and Z. Huang, Phys. Rev. ST Accel. Beams **6** 050702 (2003).
[22] M. Hogan *et al.*, Phys. Rev. Lett. **80**, 289 (1998).
[23] M. V. Yurkov, Nucl. Instrum. Methods Phys. Res. A **483**, 51 (2002).